7.4 The influence of the welding process parameters in the superconducting properties of the YBCO/Ag/YBCO joints

In Chapter 6 we have analyzed the influence of the welding parameters on the microstructure of the YBCO/Ag/YBCO joints obtained by employing a 10μm Ag foil as spacer material. In this chapter we will analyze how these parameters affect the superconducting properties of the joints, i.e. the remanent magnetization (M_{rem}) and the critical current density (J_c). The remanent magnetization of the samples studied in this work has been determined by means of the Hall probe imaging system after following a field-cooled process (fc). It depends on the geometry and on the dimensions of the samples. For instance, for comparative purposes, we have determined the critical current density of the joint and YBCO grain in order to observe which is the best configuration that we should use in order to obtain the highest quality of the joint. The methodology used to determine this magnitude has been described in Section 7.1.

7.4.1 Effect of cooling rate on the superconducting properties of the final joints

In the last chapter we have studied the influence of cooling rate on the microstructure of the final joints. It has been demonstrated that this parameter plays an important role for obtaining high quality superconducting joints. A high cooling rate has found to be detrimental for the microstructure of the final joints since non-superconducting phases such as Y211, $BaCuO_2 - CuO$ and Ag precipitates have been detected at the interface. In order to observe how the cooling rate affects the superconducting properties of the final joints we have used four different joints obtained at four different cooling rates. The samples used in this study are C_6, C_3, $C_{1.8}$ and $C_{0.6}$ (see table 6.1) which have been grown at 6, 3, 1.8 and 0.6°C/h, respectively. The dimensions of these samples are of $\simeq 1\times 1\times 0.6 cm^3$. The simplest test available with the Hall system is the remanent

Table 7.1: Dimensions of the surfaces of the YBCO monoliths submitted to the welding process and scanned by using a Hall probe. The YBCO monoliths welded of each sample studied are denoted as Grain 1 and Grain 2.

Sample code	a×b×c (Grain 1)(cm^3)	a×b×c (Grain 2)(cm^3)
C_6	1×0.49×0.6	1×0.49×0.6
C_3	1.03×0.52×0.6	0.9×0.44×0.6
$C_{1.8}$	0.95×0.5×0.6	0.95×0.45×0.6
$C_{0.6}$	0.95×0.43×0.6	0.95×0.52×0.6

magnetization map of the sample after following a field-cooled process.

For comparison purposes and a better understanding of the remanent magnetization results we present in table 7.1 the dimensions of the YBCO parts that were submitted to the welding process hereafter called Grain 1 and Grain 2, as it is schematically presented in figure 7.18. The samples studied have a similar thickness of $\simeq$ 0.6cm. Additionally, note in this table that for the samples C_3, $C_{1.8}$ and $C_{0.6}$ the dimensions of the Grain 1 and Grain 2 are slightly different. The difference in dimension of the superconducting volume of the joints could give rise to a reduction of the remanent magnetization. On the contrary, Grain 1 and Grain 2 corresponding to the sample C_6 are of similar dimensions.

In figure 7.19a it is represented a 2D remanent magnetization M=B(x,y)-μ_0H image obtained with the Hall microprobe at 77K for the sample C_6 after a field-cooled process under a magnetic field of $H_{applied} \simeq$ 5000Oe. The joint is indicated in figure by an arrow. Two differentiated peaks can be observed showing that the remanent magnetization at the joint is lower than the remanent magnetization obtained at YBCO grains. This indicates that the YBCO monoliths submitted to the welding process were weakly connected. Indeed, as it was shown in the BSE micrograph represented in figures 6.16 and 6.17b, only at the interface have been observed non-superconducting agglomerations such as Y211 phase, $BaCuO_2$-CuO phase and Ag precipitates. This explains the reduction of the remanent magnetization at the interface. The electron microprobe analysis performed on the YBCO solid matrix (see figures 6.18 (a-b)) have shown that no

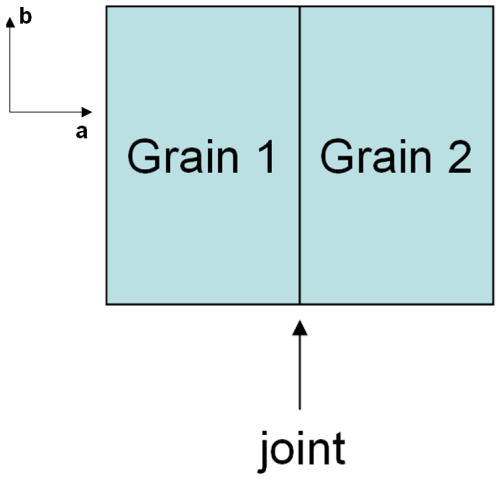

Figure 7.18: Configuration of the samples studied in this work before the welding process, were both YBCO monoliths and joint are well defined.

Ag precipitates have migrated inside and secondary phases have been formed during the welding process only at the interface.

Moreover, it can be clearly appreciated that the remanent magnetization at the left YBCO grain is M_{rem} $\simeq$3100 Gauss, while at the right YBCO grain is M_{rem} $\simeq$ 2450 Gauss. As shown in table 7.1, the dimensions of YBCO monoliths are similar which means that the difference in the remanent magnetization should be ascribed to the existence of some inhomogeneity in the YBCO grains. If we use the procedure presented in the previous section by fitting the experimental remanent magnetization profile according to the gaussian equation we obtain that the remanent magnetization profile obtained after fitting agrees well with the remanent magnetization profile obtained from experimental data (see figure 7.20). Thus, we conclude that the reduction in remanent magnetization is of $\sim$ 30%. Some differences in J_c values among both YBCO grains caused by the welding process or previously existent in the YBCO starting material is the reason for which the remanent magnetization at YBCO grains is reduced.

Figure 7.19b shows a remanent magnetization profile obtained after a field-cooled process for the sample C_3 obtained by using a cooling rate of r=3°C/h.

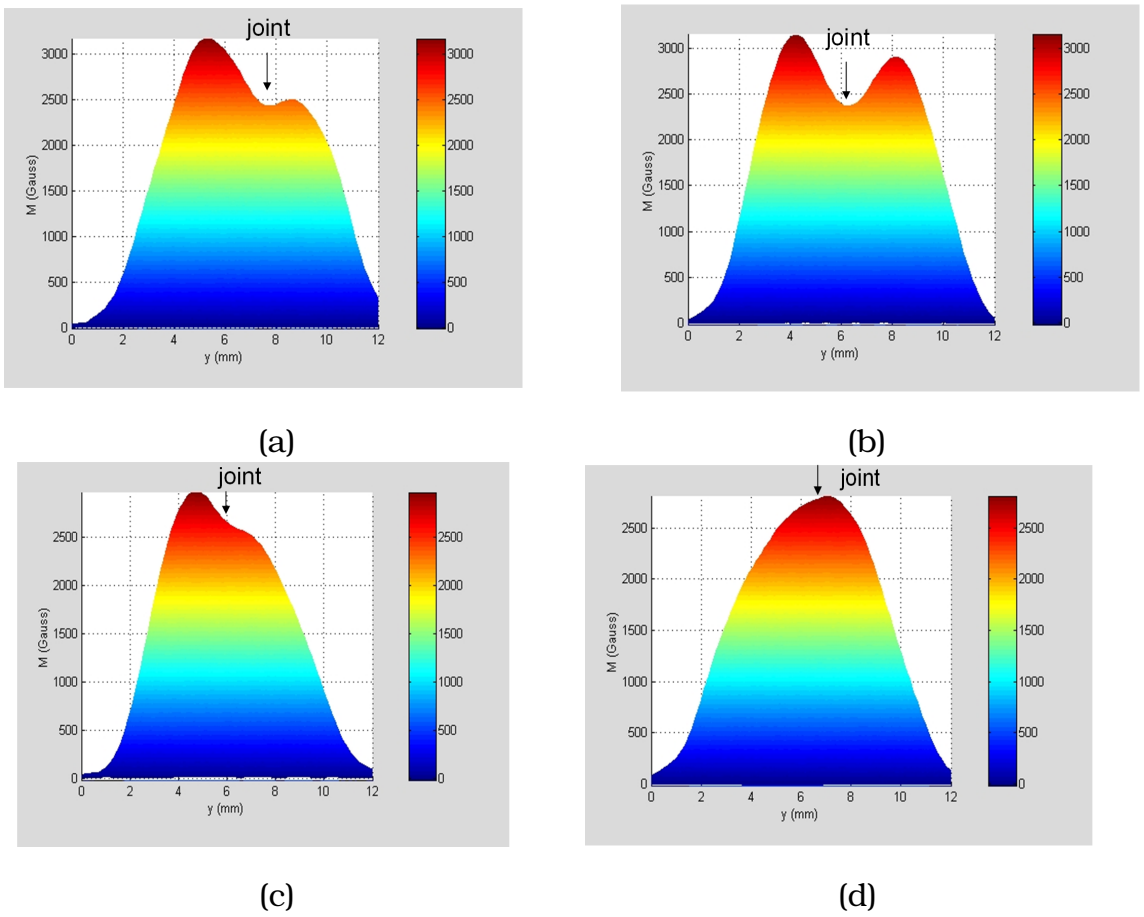

Figure 7.19: Section perpendicular to the weld of the fc remanent magnetization for:(a) C_6; b)C_3; c)$C_{1.8}$ and d)$C_{0.6}$ samples. Note that the absolute remanent magnetization of the samples is not comparable since the sample dimensions were no exactly the same.

In this case it can be observed also a double peak profile indicating that the remanent magnetization at the junction is lower than the remanent magnetization measured for the mother blocks. The remanent magnetization at the interface is M_{rem} ≃2300 Gauss. On the contrary, the remanent magnetization at Grain 1 situated in the left side is M_{rem} ≃3150 Gauss and at the Grain 2 from the right side M_{rem} ≃2860 Gauss, which indicates a small inhomogeneity in the remanent magnetization of the mother blocks. Note in table 7.1 that one grain has a lower superconducting volume than the other. In order to see if the difference in superconducting volume of YBCO grains submitted to the welding process is the

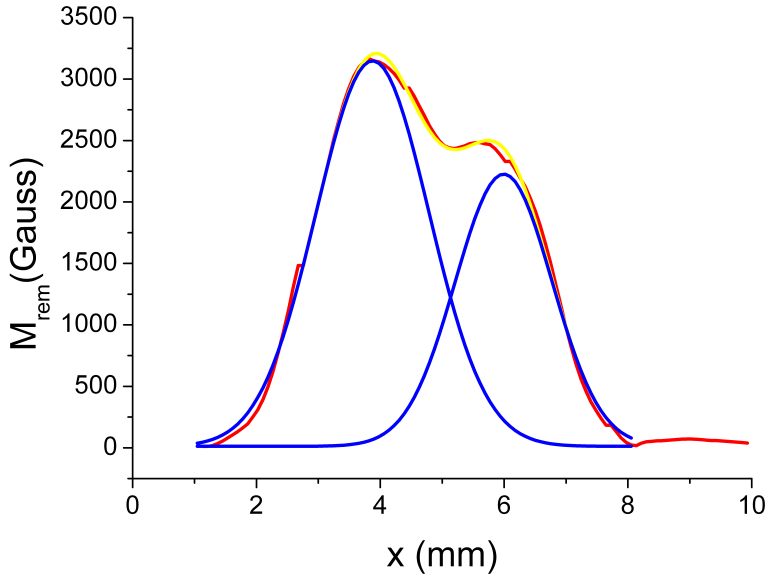

Figure 7.20: Red line: Section of the remanent magnetization profile obtained for the sample C_6. Blue lines: Remanent magnetization profile obtained for each YBCO grain after the fitting of experimental data. Yellow line: Sum of remanent magnetization profiles corresponding to YBCO grains.

reason for which takes place the reduction in remanent magnetization, we will treat both YBCO grain separately, as two samples. If the reduction in remanent magnetization is calculated in the assumption that both YBCO grains exhibit the same critical current density, we obtain that the ratio M_1/M_2 is $\sim$10%. To determine this ratio M_1/M_2 from the experimental data we should ensure the separation of remanent magnetization contribution of the joint from the remanent magnetization distribution of YBCO grains. This separation has been done by fitting the section of remanent magnetization profile in a gaussian (equation 7.1).

In figure 7.21 it is shown by red line the experimental remanent magnetization profile, by blue lines the remanent magnetization profile corresponding to each YBCO grain after the fitting and the elimination of remanent magnetization contribution of the joint and by yellow line the sum of both remanent magneti-

zation profiles after fitting. The good agreement between the experimental data and the fit suggests that remanent magnetization contribution of the junction does not affect the contribution of the grains at the maximum value of M. From experimental data we obtain that the reduction in remanent magnetization is ∼7%. This means that indeed both YBCO grains exhibit the same superconducting properties and that the reduction in remanent magnetization is mainly due to the difference in superconducting volume. Since the microstructural studies of this sample regarded in figure 6.19 and the electron microprobe analysis regarded in figures 6.21(a-b) had shown the existence of non-superconducting phases at the interface, the reduction of remanent magnetization at the interface with respect with the remanent magnetization obtained for YBCO grains is expected.

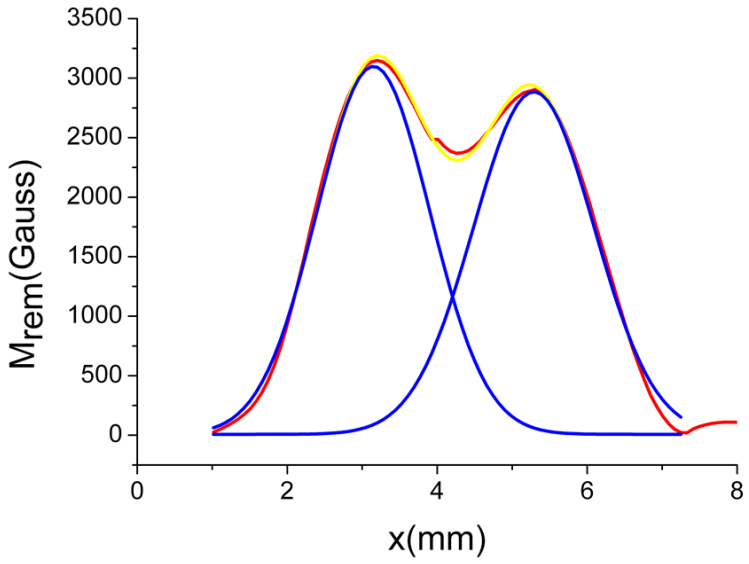

Figure 7.21: Red line: Section of the remanent magnetization profile obtained for the sample C_3. Blue lines: Remanent magnetization profile obtained for each YBCO grain after the fitting of experimental data. Yellow line: Sum of remanent magnetization profiles corresponding to YBCO grains.

A clear improvement of the quality of the superconducting joint can be observed when the cooling rate is decreased down to r$\leq$ 1.8°C/h. Note in figures 7.19(c-d) that the remanent magnetization map presents two less differentiated peaks indicating a small reduction of J_c at the joint area when the cooling rate r=1.8°C/h is investigated and only one peak for the sample $C_{0.6}$ grown at a cooling rate of r=0.6°C/h, respectively, as it is typically observed for a single domain showing that the YBCO monoliths submitted to the welding process are strongly connected. In the remanent magnetization profile corresponding to the sample $C_{1.8}$ we can appreciate that the YBCO grains exhibit a slightly different remanent magnetization values in their center. This is probably due to a different J_c among both YBCO grains. The asymmetry could be interpreted as a result of some differences between the superconducting volume of both grains or to some pre-existing inhomogeneities in the YBCO monoliths. The microstructural studies performed on the ab plane of this sample, had shown that some phases have been found at the edge of the interface at the upper part of the interface. Observe in figure 6.22 that it seems that non-superconducting phases have been formed or have been existed from the starting material in the upper part of the interface. The existence of these phases inside the grain from the upper part reduces its superconducting volume in which the supercurrents flow up to $\simeq$15% with respect to the superconducting volume which exhibits the grain from the lower part. Thus, the reduction in remanent magnetization is 8% if it is calculated by using the equation 2.4 and 7% if it is calculated from the experimental data. The similarity between the ratio M_1/M_2 calculated in two ways make us conclude that the reduction in remanent magnetization profile is mainly due to the difference in superconducting volume of the YBCO grains. However, in this case, the reduction of superconducting volume of one grain with respect to the other is due basically to the inhomogeneity found at the edge of the interface. In this case, if we compare the remanent magnetization at the interface with the remanent magnetization corresponding to the grain from the right side,

the difference is negligible. Concerning the asymmetry found in the remanent magnetization profile of the sample $C_{0.6}$, we can conclude that is due to the differences in superconducting volume of both YBCO grains submitted for joining since the right-hand grain (Grain 1) was a surface scanned by the Hall probe of 0.95×0.43cm^2, the left-hand grain (Grain 2) was a surface of 0.95×0.52 cm^2. The thickness of the sample is the same ≃0.6cm.

The remanent magnetization studies give a qualitative idea of the current flow in the whole bulk sample. However, in order to have a quantitative information about the distribution of currents over the sample, and about the absolute magnitude of the critical current density, the current maps associated to the remanent magnetic flux were computed using the software package "Caragol". As it has been explained in Chapter 3, the program basically solves the inverse problem in a "quasi" 3-D mode, but no assumption on the contour of the sample is taken.

The critical current density of both YBCO grains and the joint as function of the cooling rate are represented in figure 7.22. The error bars show the inhomogeneities in J_c's values found for all three parts of the samples analyzed. The red symbols indicate the J_c^{grain1} values, the blue symbols the J_c^{grain2} values and the yellow ones the J_c^{gb} values. Observe that YBCO grains submitted to the welding process to obtain the final joints C_3 and C_6 are considered to have similar superconducting properties since the error bars in the figure are overlapping. The dispersion of J_c values is mainly due to the inhomogeneity existent in the proper grain. On the contrary, observe in the figure that YBCO grains used to obtain the final joints $C_{0.6}$ and $C_{1.8}$ are not considered to have a similar critical current density since the error bars are not overlapping, especially for the sample $C_{0.6}$. For these two samples, observe too that the difference between the lower J_c value corresponding to the YBCO grains and J_c^{gb} values is practically negligible. From a quantitative point of view, we can conclude that: J_c^{gb} of the sample $C_{0.6}$ is of ≃1.35×10^4A/cm^2 and of the sample $C_{1.8}$ is of ≃1.18×10^4A/cm^2.

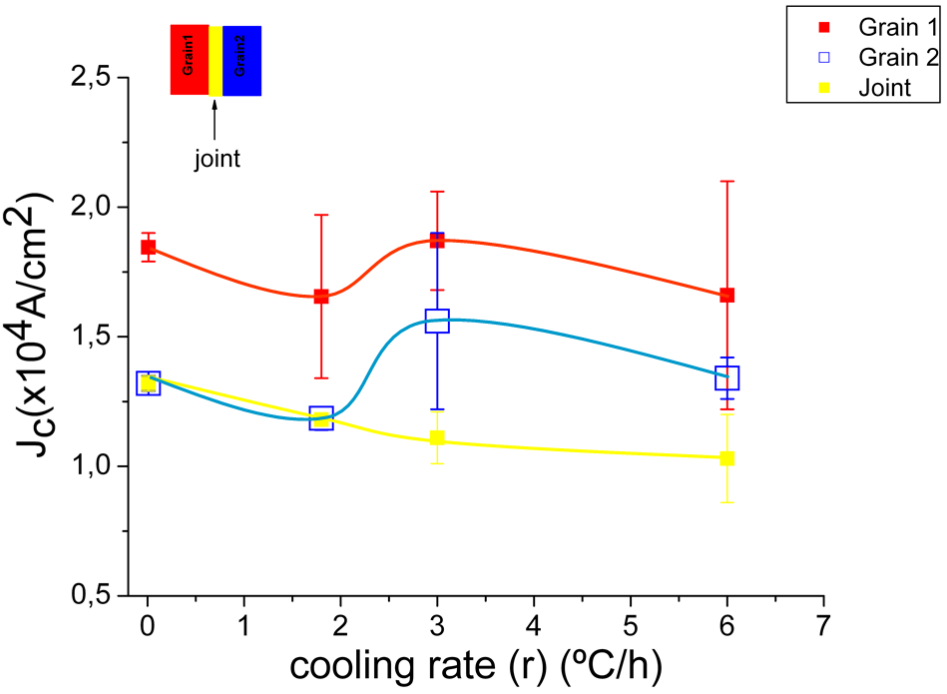

Figure 7.22: Dependence of critical current density on the cooling rate for: Grain 1 (red symbols), Grain 2 (blue symbols) and for the joint (yellow symbols). The error bars quantify the dispersion of J_c values.

For a better correlation of the superconducting properties of the joints with their microstructure, the calculated current distributions obtained from the Hall magnetic flux map in the remanence after a field cooled process of all the samples studied in this section, are presented in figures 7.23 (a-d). The position of the weld and the sample limits are indicated for clarity. Note that when the cooling rate is high, i.e r$\geq$3°C/h, the distribution of the current calculated reflects clearly the inhomogeneities found at the interface and the differences in the YBCO grains as can be observed in figures 7.23(a-b). For the sample C_6 it can be appreciated three induced current loops corresponding to the circulation of one intergrain current associated to the current which flows across the joint and two intragrain currents associated to the currents which flow within the

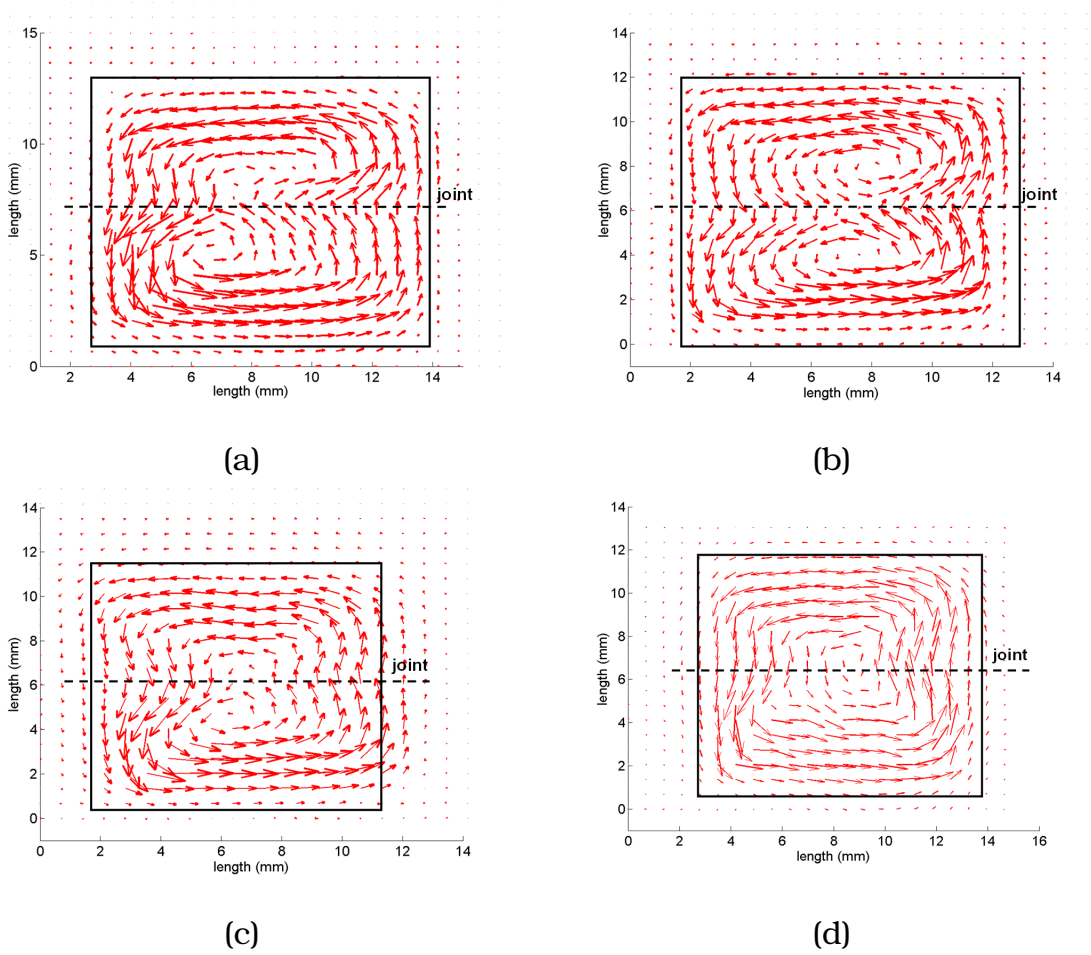

Figure 7.23: Current distribution calculated from Hall magnetization map in the remanence after a fc process of the samples: a)C_6, b)C_3, c)C_{18}, d)C_{06}. The position of the weld and the sample limits are indicated in the figure for clarity.

grains. When the microstructure of the sample C_6 was investigated (see figure 6.16 located in Chapter 6), it was clearly noticed that some non-superconducting phases containing Ag-rich liquid, $BaCuO_2$-CuO and Y211 phases have been trapped at the junction. The same weak link behavior was observed for the sample C_3. As in the previous case, the current penetrates faster the joint than the YBCO grains, indicating the low quality. If we correlate the distribution current pattern with the microstructure of the ab plane of this sample shown in figure 6.16 from Chapter 6 we can conclude that the reduction of J_c is associated with

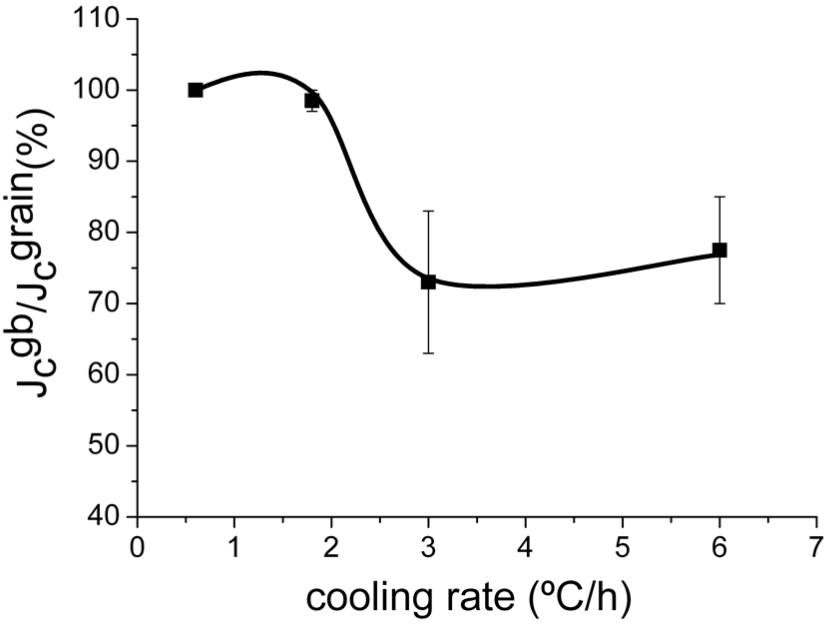

Figure 7.24: Dependence of ratio J_c^{gb}/J_c^{grain} with the cooling rate.

the existence of these non-superconducting phases detected at the interface by WDS analysis.

The presence of some inhomogeneities at the interface of the sample $C_{1.8}$, has given place to a small reduction in the J_c values of the junction (see figure 6.22). Because of this, the current pattern exhibits two current loops. It can be clearly observed in the critical current density pattern distribution that the lower part of the sample exhibit higher J_c values than the rest of the sample which agrees with the results obtained from microstructural analysis. On the contrary, in figure 7.23d corresponding to the sample $C_{0.6}$ note that only a single circulation loop over the whole sample is seen, which is hardly indistinguishable from that of a bulk sample. This result fully agrees with the microstructural analysis which showed a clean and crystallographic incident interface (see figure

6.25 represented in Chapter 6). This confirms the success of our new technique to produce high critical current density welds in YBCO bulk materials.

A small inhomogeneity is found in the J_c^{gb}/J_c^{grain} values for the welds cooled at r<1.8°C/h as indicated by the error bars shown in figure 7.24. The critical current densities of these joints are hardly decreased as compared with the critical current density of the YBCO material. It is interesting to observe that the J_c^{gb} of the joint did not decrease compared with the J_c^{grain} when the cooling rate was of 0.6°C/h. On the other hand, when the cooling rate is increased to 3°C/h or 6°C/h it is found that the ratio J_c^{gb}/J_c^{grain} is substantially reduced. Thus, the critical current density at the weld is reduced by 25%-27% from that of the respective YBCO single domains. Additionally, the error bars in the graph show that the inhomogeneity in the proper material is even much bigger than in the previous cases. These results are in concordance with the results obtained from the microstructural analysis (see figures 6.16 and 6.19). Because of the pushing effect, Ag liquid is pushed from the center of the junction to its edges by the growing fronts. Too high cooling rate did not allow the complete elimination of the liquid which has been trapped at the interface. It is known that this kind of phases deteriorate drastically the superconducting quality of the joints, which is confirmed by our experiments.

In figure 7.25 it is represented the dependence with the cooling rate of the angle α determined from J_c^{gb}/J_c^{grain} values according to the equation 7.1. For all the samples analyzed the angle obtained is below 33º. This result suggests that even if the cooling rate employed was too high, the final joints do not reach the poor quality of the glued-sample. As the cooling rate increases, α increases too, indicating a decreasing of the critical density of the joint with respect to the critical current density of the weakest YBCO grain. When the cooling rate is r=0.6°C/h, α=0º, i.e. J_c^{gb}=J_c^{grain}. As it was mentioned in Section 7.1, when the J_c^{gb} exhibits the same value as J_c^{grain}, the pattern of stream lines should be similar to the pattern predicted by this model for a rectangular shape sample.

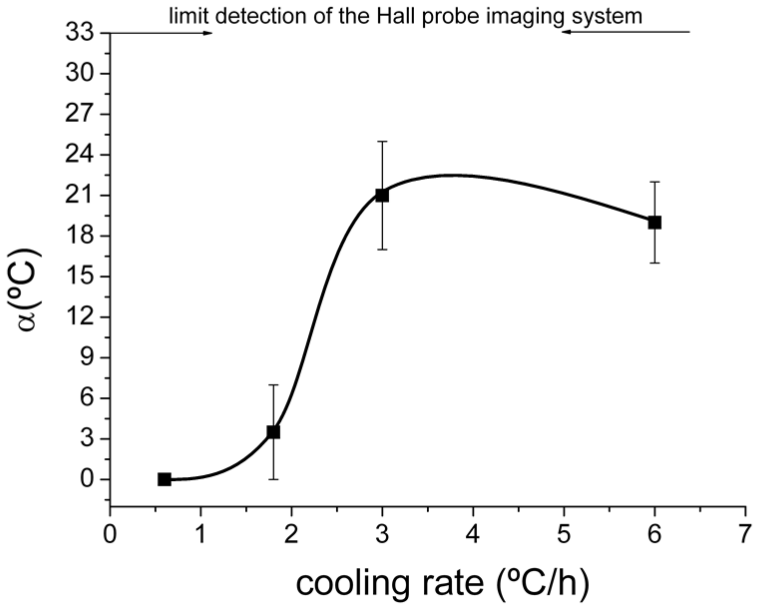

Figure 7.25: Dependence with the cooling rate of angle α which describes the angle between d^+ lines and the junction line. The limit detection of the Hall probe imaging system used is indicated in the figure.

Indeed, if we compare the pattern obtained experimentally and indicated in figure 7.23d with the theoretical pattern shown in figure 7.1b we can observe a similarity suggesting once again that the optimum cooling rate needed to obtain artificial joints without any decrease in critical current density at the junction is r=0.6°C/h. Note in the figure that if r=6°C/h, α is spanning between 16° and 19°, if r=3°C/h between 17° and 25°, and if r=1.8°C/h between 0° and 7°

7.4.2 Effect of temperature window on the superconducting properties of the final joints

Joints grown at different temperature windows are studied in this section in order to see how this parameter affects the superconducting properties of the final joints. In Chapter 6 their influence on the microstructure it has been

studied. In figure 6.15 shown in Chapter 6 it is represented the welding process which was employed in order to obtain the joints presented in this study. The parameters used were T_{max}=992°C, t_1=3hours, T_2=973°C, t_2=1h, r=0.6°C/h, t_{ox}=168-240°C and T_{ox}=450°C being the values which up to now allowed us to obtain joints with high critical current densities. The parameter T_3 is investigated in this section, being the temperature that determines the temperature window. We have studied three different samples grown in a temperature window of 28, 23 and 18°C and cooled down from T_2=973°C using a cooling rate of 0.6°C/h, i.e. the cooling rate which exhibits the best behavior from the point of view of the microstructural and superconducting properties.

Thus, the superconducting behavior of the samples ΔT_{28}, ΔT_{23} and ΔT_{18} is studied by determining the remanent magnetization after a fc process and the critical current density of the joints. In table 7.2 are reported the dimensions of the YBCO surfaces of the single domains that were welded and, then, scanned by using the Hall probe system. As it was previously mentioned, the remanent magnetization depends on the transverse dimensions of the studied samples. Therefore, for comparison purposes, it is important to know the dimensions of each YBCO monolith used for the welding process. Note in table 7.2 that the dimensions of the YBCO grains submitted to the welding process and corresponding to the sample ΔT_{28} are similar, whereas for the rest of the samples are slightly different. The difference in superconducting volume gives rise to a reduction in remanent magnetization of the YBCO grains as it was observed before.

Figures 7.26 (a-c) show the remanent magnetization map after a fc process of the samples ΔT_{28}, ΔT_{23} and ΔT_{18}, respectively. The applied magnetic field was $H_{applied}\simeq$5000 Oe and it was parallel to the c-axis of the single domain and parallel to the joint. The first observation concerning the remanent magnetization profiles is that the temperature window indeed affects the superconducting quality of the samples. The reduction of the remanent magnetization at the junction

Table 7.2: Dimensions of the surfaces of the YBCO monoliths submitted to the welding process and scanned by using a Hall probe. The YBCO monoliths welded of each sample studied are denoted as Grain 1 and Grain 2.

Sample code	a×b×c (Grain 1)(cm^3)	a×b×c (Grain 2)(cm^3)
ΔT_{28}	0.43×0.95×0.6	0.52×0.95×0.6
ΔT_{23}	0.44×1×0.6	0.56×1×0.6
ΔT_{18}	0.47×0.97×0.6	0.5×0.97×0.6

with respect to the YBCO grains, indicates a low critical current density of the joint when compared with the critical current density of the YBCO grains and could be associated with the presence of some inhomogeneities formed during the welding process. The highest reduction takes place for a low temperature window ΔT=18°C. When ΔT=28°C, only one peak can be observed indicating that the remanent magnetization at the junction is not decreased during the welding process. On the contrary, the remanent magnetization profiles corresponding to the samples ΔT=23°C and ΔT=18°C present a double peak. The reason of the degradation of the weld can be found in the microstructural studies of the respective samples. In Chapter 6 it has been shown that indeed, the microstructure is affected by the temperature window. Figures 6.39(a-b) and 6.40(a-b) corresponding to the ab and ac planes of the samples Δ_{18} and Δ_{23}, respectively, have shown that when the joints are grown in a small temperature window, residual liquid phases corresponding to a mixture of Y211 particles, Ag precipitates and $BaCuO_2$-CuO phase have been trapped at the interface. This means that the liquid could not be completely solidified and that Ag did not have time to be pushed away outside the interface during the slow cooling time.

Note that when the sample is grown in a temperature window of ΔT=23°C or ΔT=18°C, the remanent magnetization profile exhibits a double peak behavior and a consistent difference between the remanent magnetization values corresponding to YBCO grains. As shown in the table, the dimensions of the YBCO parts are slightly different, as a consequence, we could attribute the difference

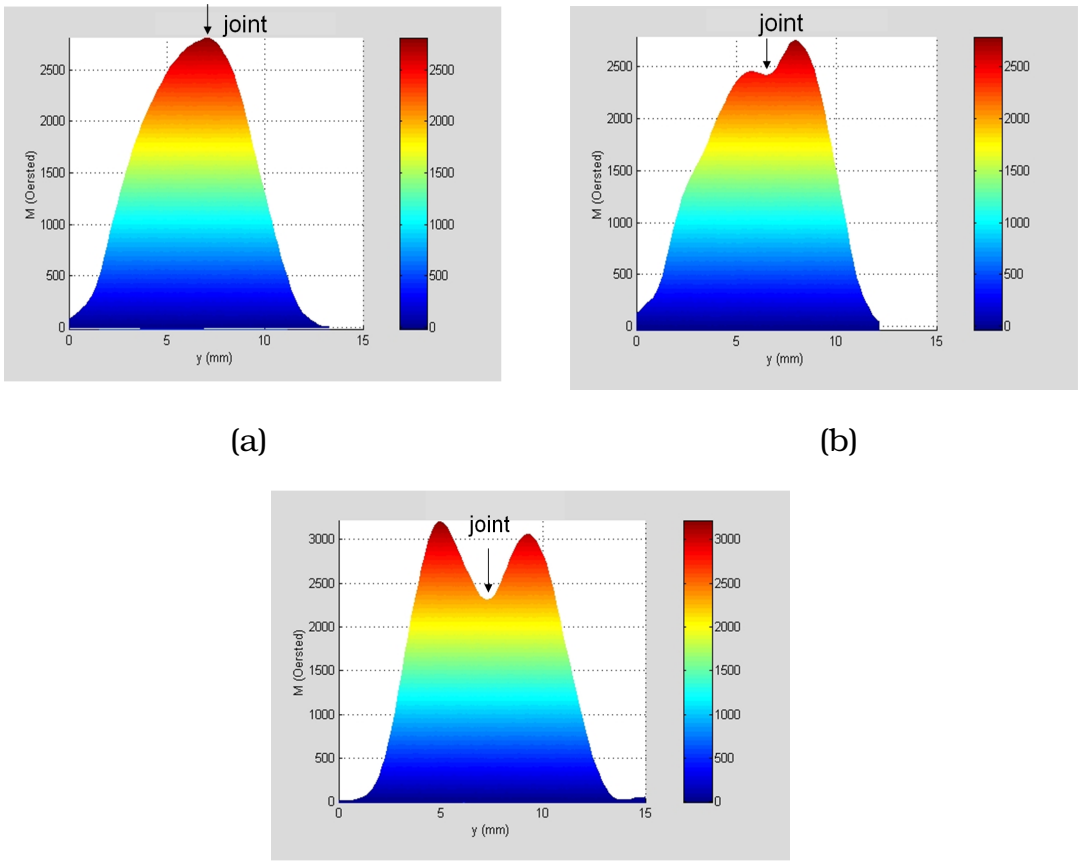

Figure 7.26: 2D remanent magnetization map after a fc process for:(a) ΔT_{28}; b)ΔT_{23}; c)ΔT_{18}. Note that the absolute remanent magnetization of the samples is not comparable since the sample dimensions were no exactly the same. The joint is indicated by arrow.

in the remanent magnetization profile to the difference in superconducting volume. For both samples, we have fitted the remanent magnetization profiles to the Gaussian equation 7.1. In figures 7.27 and 7.28 are shown the fits obtained for samples ΔT=18°C and ΔT=23°C, respectively. When the sample ΔT=18°C is investigated observe that the fit is adjusted to the experimental profile. Thus, the calculated reduction of remanent magnetization due to the difference in volume is M_1/M_2 is ∼5% and determined from experimental data is 4.5%. The values obtained are similar, therefore, we can conclude that the reduction in remanent magnetization is mainly due to the difference in superconducting volume

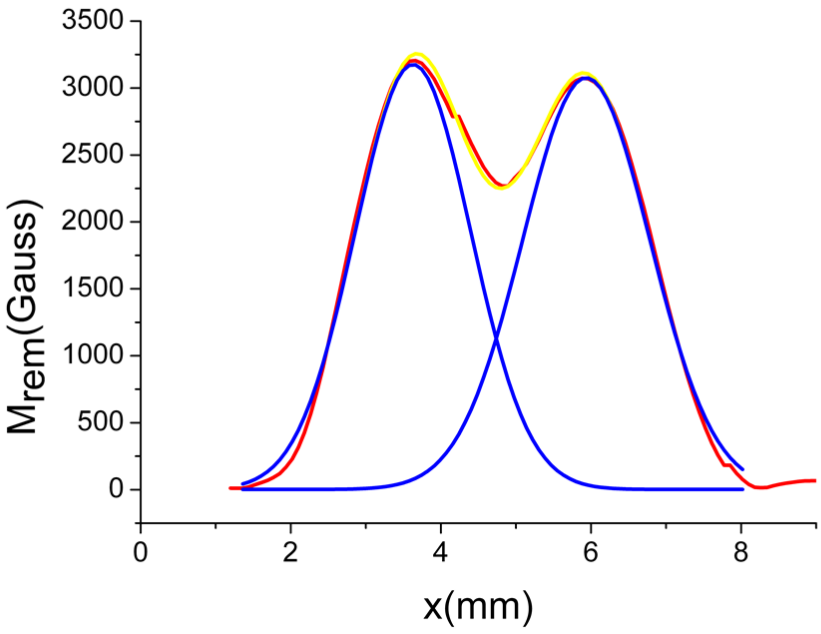

Figure 7.27: Red line: Section of remanent magnetization profile corresponding to the sample Δ_{18}; Blue lines: Remanent magnetization profile corresponding to each YBCO grain if it is analyzed separately after a gaussian fit of the experimental profile. Yellow line: Sum of remanent magnetization profiles obtained after the gaussian fit.

of YBCO grains submitted to the welding process. On the contrary, for the sample ΔT=23°C, note that a small difference is obtained between the fit and the remanent magnetization profile obtained from experimental data. Because both peaks associated with the remanent magnetization at the YBCO grains are quite close, the remanent magnetization contribution of the junction influence the remanent magnetization contribution of the grains and cannot be completely separated. Because of this, after the gaussian fit the remanent magnetization corresponding to both are substantially reduced, when they are treated separately. In this case the reduction in remanent magnetization calculated from equation 7.1 and assuming that both YBCO grains have the same critical current density, is 15%, whereas when it is calculated from the experimental data

is 27%. The assumption made in order to determine the reduction in remanent magnetization is not very clear in this case, since the separation of contributions is not complete after the fitting.

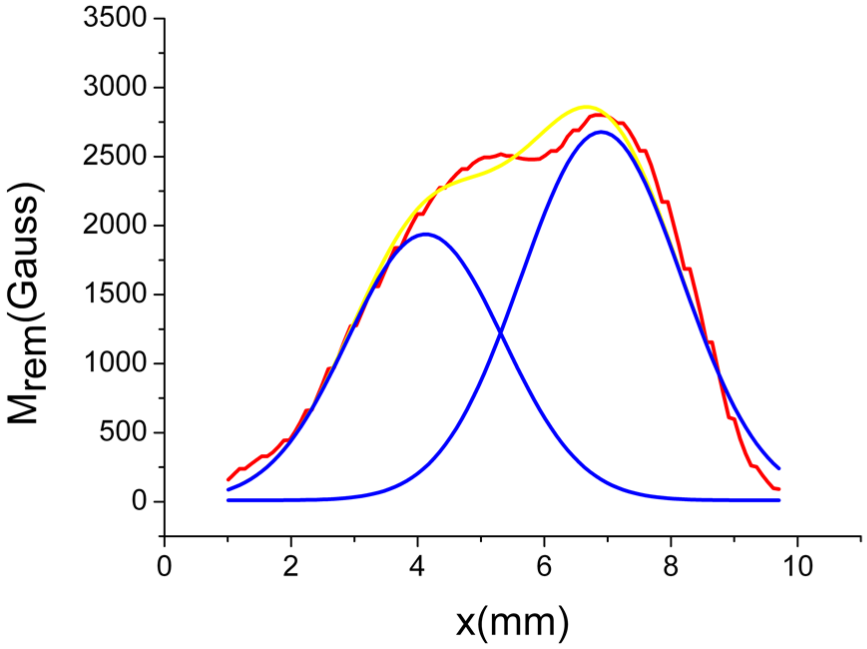

Figure 7.28: Red line: Section of remanent magnetization profile corresponding to the sample ΔT_{23}; Blue lines: Remanent magnetization profile corresponding to each YBCO grain if it is analyzed separately after a gaussian fit of the experimental profile. Yellow line: Sum of remanent magnetization profiles obtained after the gaussian fit.

Circulating current vectors calculated from the distribution of the remanent magnetization in the samples studied in this section after the fc process are represented in figure 7.29(a-c). Calculated critical current density distributions of a good quality weld from a field-cooled process show a single circulation loop over the whole sample which is typically indistinguishable from that of un-welded samples (see figure 7.29a). Observe that for the sample ΔT_{28}, circulating current vectors form a rectangular-shaped distribution, associated with the X-cross geometry of the growth sectors generated during the top seeding growth pro-

cess [100]. Thus, this sample behaves like an YBCO single-domain without the presence of any defects at the junction. Indeed, if we compare the calculated current pattern obtained for this sample with that obtained for a rectangular-shaped single domain presented in figure 7.1, a strong similarity is observed. On the contrary, for samples grown in lower temperature windows, the calculated current density distributions (see figures 7.29(b-c)) show three current loops, two of them corresponding to the current flowing within the grains and one corresponding to the current flowing across the junction. The existence of three current critical density loops indicate the weak link behavior of the YBCO joints.

In figure 7.30 are represented the critical current density values for each part of the samples studied: Grain 1 (red symbols), Grain 2 (blue symbols) and joint (yellow symbols) for each temperature window. Observe that the error bars corresponding to Grain 1 and Grain 2 of samples ΔT_{18} and ΔT_{23} are overlapping meaning that the inhomogeneity in J_c values is mainly due to some inhomogeneity exhibited by the proper grains, not by differences in microstructure between the both YBCO grains. On the contrary, the error bars associated with YBCO grains corresponding to the sample ΔT_{28} are not overlapping. Thus, we can conclude that this sample exhibits YBCO grains with inhomogeneities. The critical current density of the joint is spanning between $1.28 \times 10^4 A/cm^2$ and $1.35 \times 10^4 A/cm^2$ when the temperature window was of 28°C, between $1.03 \times 10^4 A/cm^2$ and $1.3 \times 10^4 A/cm^2$ for a temperature window of ΔT=23°C and between $1 \times 10^4 A/cm^2$ and $1.22 \times 10^4 A/cm^2$ for a temperature window of ΔT=18°C. The respective YBCO grains exhibit values between $1.28 \times 10^4 A/cm^2$ and $1.9 \times 10^4 A/cm^2$ for the sample ΔT_{28}, between $1.17 \times 10^4 A/cm^2$ and $1.83 \times 10^4 A/cm^2$ for the sample ΔT_{23} and between $1.46 \times 10^4 A/cm^2$ and $2.1 \times 10^4 A/cm^2$ for the sample ΔT_{18}. In order to observe the percentage of reduction of critical current of the joint with respect of the YBCO grain we will analyze the ratio J_c^{gb}/J_c^{grain}.

In figure 7.31 it is shown the dependence of ratio J_c^{gb}/J_c^{grain} with the temperature window. The error bars in the figure quantify the dispersion of the J_c^{gb}/J_c^{grain}

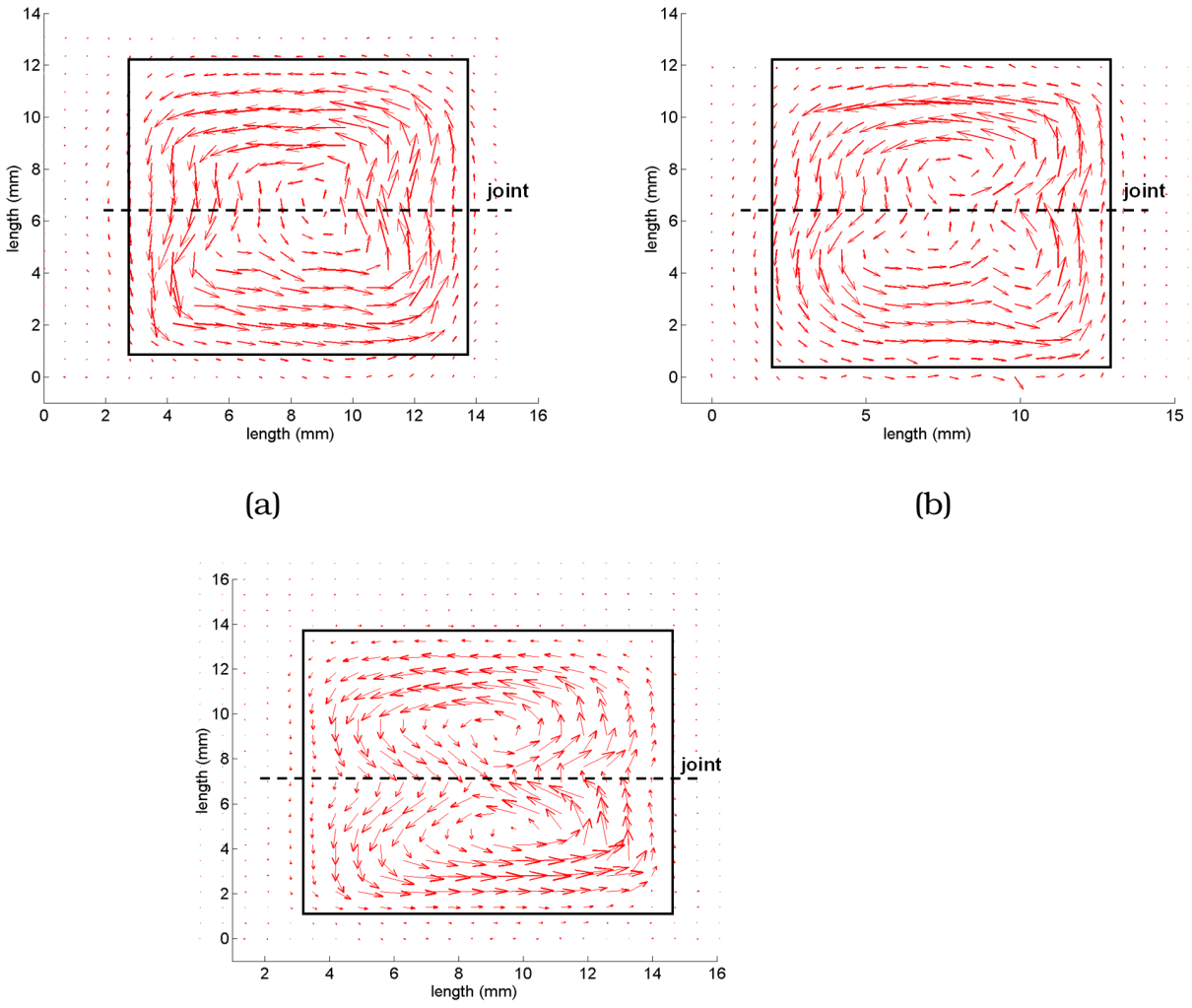

Figure 7.29: Circulating current vector calculated from flux mapping shown in figure 7.26(a-c) corresponding to the samples: a)ΔT_{28}, b)ΔT_{23} and c)ΔT_{18} respectively. The sample limits and the junction are shown in figure for clarity.

values obtained by employing the methodology proposed by us to determine the critical current density of the final joints. The highest value of this ratio is obtained for the sample ΔT_{28} grown employing a slow cooling rate of r=0.6°C/h in the temperature window of ΔT=28°C. In this case, no reduction of the critical current density of the joint when compare with the J_c^{grain}. On the contrary, when

the samples ΔT_{23} and ΔT_{18} are investigated, the critical current density of the joint is reduced.

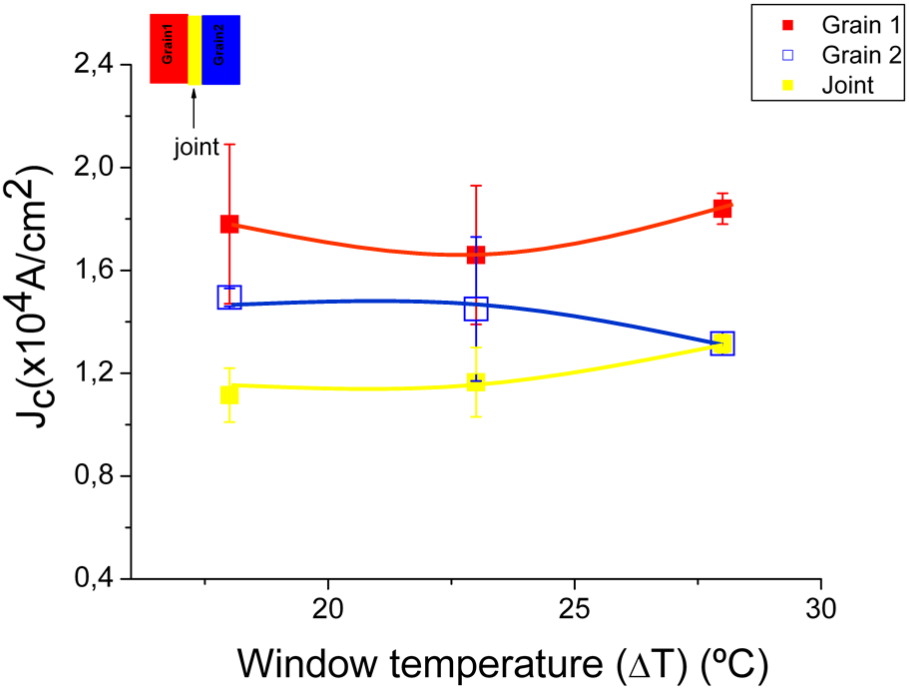

Figure 7.30: Critical current density values corresponding to the Grain 1 (red symbols), Grain 2 (blue symbols) and joint (yellow symbols) for each temperature window investigated.

At the beginning of this Chapter it was shown that the line on which the magnetization currents sharply change direction and the joint line form an angle α given by the equation 7.1. For instance, this angle depends on the ratio J_c^{gb}/J_c^{grain}. In order to determine this angle we will calculate the ratio J_c^{gb}/J_c^{grain} for all the samples studied, by employing the methodology described in Section 7.1. In this way we can conclude which is the best configuration we should use in order to obtain the highest joint quality. As it was mentioned, higher α implies a decreasing of the ratio J_c^{gb}/J_c^{grain}. As shown in the figure, when ΔT=18°C the angle α is spanning between 18º-23º, when Δ=23°C α is spanning between 14º-20º and when ΔT=28°C α=0º. For the samples ΔT_{18} and ΔT_{23}, the current

penetration through the joint is faster than the penetration inside the YBCO grains. This means that the critical current density of the joint is lower than the critical current density of the YBCO grains. Moreover, observe in figures 7.29(b-c) that when the current lines reach the center of the sample, closed current loops are formed inside the grains indicating once again the weak link behavior of the joint. This reduction of the critical current density resides in the existence of non-superconducting phases formed during the welding process and detected by microstructural analysis in Chapter 6. In these analysis has been observed that when the joints are grown in a small temperature window, Ag liquid could not be eliminated completely outside the interface. And because of the small temperature window Ag-rich liquid did not have time for solidification. On the contrary, when the sample ΔT_{28} was investigated only one current loop was observed inside the sample. Thus, we can conclude that this sample acts as one grain without any reduction of the critical current density at the junction. Indeed, if α=0, the current distribution profile should be similar to the current distribution profile obtained for a rectangular sample represented in figure 7.1.

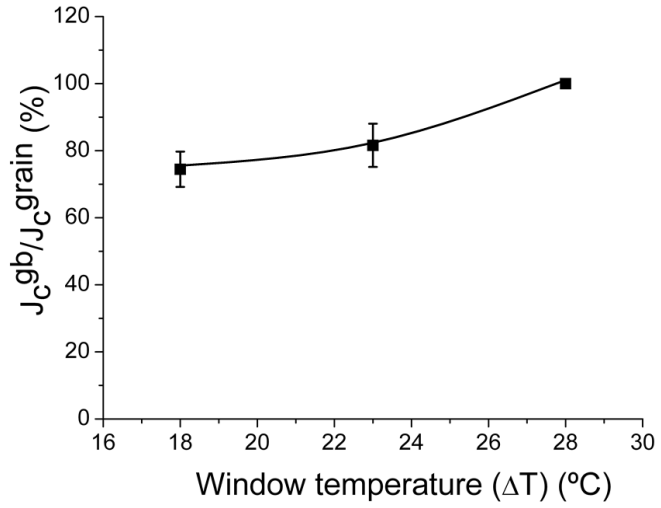

Figure 7.31: Dependence of ratio J_c^{gb}/J_c^{grain} with the temperature window.

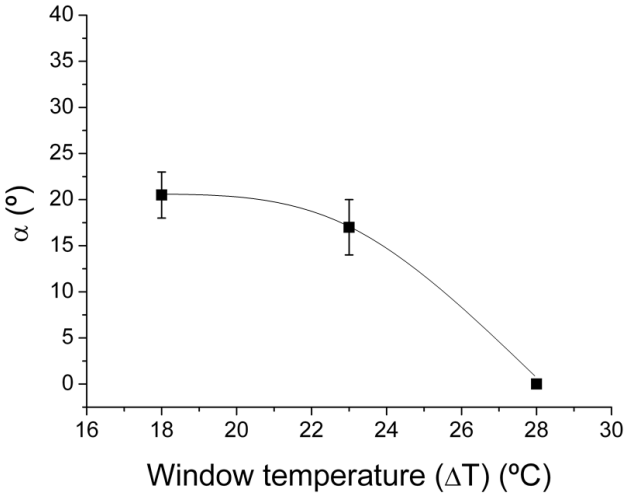

Figure 7.32: Dependence of the angle α with the temperature window.